Acoustic Reflectometry for Pitot Tube Blockage Detection

J. Rodrigues[a], S. Grey[b], M. Azarpeyvand[c] and T.C.S. Rendall[d]

Faculty of Engineering, University of Bristol, BS8 1TR, U.K.

Experimental and numerical acoustic results for Pitot tubes are presented to explore the theoretical basis for an acoustic blockage detection system. Three Pitot-statics from two different commercial aircraft were CT scanned to determine their internal geometry, and a finite element acoustic study was performed to determine the variation between blocked and unblocked reflected acoustic waves when subjected to a sinusoidal input. To validate this, supporting experiments were conducted on the same tubes when subjected to a range of blockage types, including tape, pre-deceased insects, foam, and metal. Experimental and numerical results confirm acoustic detection of all tested blockages is feasible in a quiet environment, for both the total and static pressure measurements, but only if the pressure line forms a clean waveguide along its length. The frequency range for detection is specific to each of the two Pitot designs, but a common feature is that the blocked/unblocked variation diminishes as frequency is raised due to an increase of impedance with frequency. A current limitation of the method is that is has not yet been shown to be operable in flight.

I. Introduction

Pitot tubes, devised originally by Henri Pitot in 1732 for measuring flow rates in the river Seine [1], are instruments used to measure local flow speed. Subsequently Pitot tube design was revised to its approximate current form by Henry Darcy in the mid-19$^{\text{th}}$ century [2]. Pitots are presently used for aviation, weather and industrial applications. In aircraft, airspeed is calculated from total and static pressure measurements obtained at the respective ports (Fig. 1(a)). In Pitot-static tubes, there is a large port in the direction of the flow that measures the total pressure, termed the Pitot head, and multiple smaller static pressure ports perpendicular to the flow.

The Pitot for a commercial aircraft is very far from being a simple bent tube. It must handle icing through a heating element, avoid water ingress through a chamber and baffle system, together

[a] PhD Student, Department of Engineering, University of Cambridge. Work was conducted as MEng Research Student, Department of Aerospace Engineering, University of Bristol. AIAA student member.
[b] PhD Student, Department of Aerospace Engineering.
[c] Senior Lecturer, Department of Mechanical Engineering. Royal Academy of Engineering Research Fellow.
[d] Lecturer, Department of Aerospace Engineering. Member AIAA.

with drain holes and a water trap, and provide accurate results despite interference from the fuselage pressure field. It also needs to compensate for yaw and pitch angles that might otherwise degrade accuracy. It needs to work across the full Mach number range, and ideally should require little maintenance. Pitots are therefore highly evolved instruments, certified and tested throughout their operational envelopes. While alternative systems exist, or are being developed to offer complementary or even a replacement measuring capability, it appears likely Pitots will remain the basis of airspeed measurement for many years. Despite the possibility of blockage, Pitots are reliable, cheap and thoroughly understood.

The blockage risk is, however, costly in lives. Since 1974, Pitot or static system blockages have been a played a role in accidents resulting in 564 deaths in commercial aviation. The 2009 Air France 447 accident most recently focused public attention, but unfortunately the history of accidents linked to Pitots is as old as aviation itself. From an engineering perspective, a single Pitot failure is relatively minor since they are usually mounted in triplicate on large aircraft. However, failure of all three still allows an aircraft to safely land, albeit with a non-standard flying procedure. Technically, a more serious situation arises when static ports are obstructed, denying altitude and vertical speed information, in addition to airspeed. Accidents where behaviour of the Pitot-static system was involved in some way include:

- Air France Flight 447 – June 1st, 2009: A330 lost speed indication after entering a thunderstorm at cruise altitude, triggering a chain of events that led to an aerodynamic stall [3].
- Austral Lineas Aereas Flight 2553 – October 10th, 1997: due to ice formation inside the Pitot of the DC-9, the airspeed indicated fell to low levels, prompting increases in thrust and extension of slats. As a consequence of the excessive aerodynamic forces, one of the slats tore from the aircraft, causing severe asymmetry and loss of control [4].
- Aeroperú Flight 603 – October 2nd, 1996: static ports were blocked by tape. This led to a total failure of multiple flight instruments and due to the false data presented and associated loss of situational awareness the aircraft flew into the sea [5].
- Birgenair Flight 301 – February 6th, 1996: the aircraft had remained unused for some time. A Pitot tube blockage, likey caused by an insect nest, led to erroneous measurements and initiated crew confusion that culminated in a crash [6].
- Northwest Airlines Flight 6231 – December 1st, 1974: in-flight icing of Pitot tubes provided erroneous airspeed data, leading to a stall and loss of the aircraft [7].

There have also been other cases where inaccurate airspeed data led to flight incidents without fatal outcomes, such as the Rockwell X-31 accident (January 19th, 1995) where icing of the Kiel probe (a type of shrouded Pitot) gave incorrect airspeed to the autoflight system, which then used inappropriately high control law gains, causing aircraft divergence. The pilot managed to eject and

the aircraft crashed [8]. Further examples in commercial aviation are reported by the US National Transportation Safety Board [9, 10] and the UK Air Accident Investigation Branch [11].

From a piloting point of view, a Pitot failure is much more serious than might be expected, as it often triggers a human and/or automated chain of events significantly more difficult to arrest. Pitot discrepancies are only obvious during the takeoff roll, which is a poor moment to resolve apparent errors between three measurements or make decisions based upon them. A complete failure of the static system can easily be fatal, as for Aeroperú 603, depending on availability of any other visual cues. Even failure of a single Pitot, or temporary failure of all three, can lead to a fatally confusing situation, as for Birgenair 301 and Air France 447. Fundamentally, if blockages can be detected, subsequent piloting decisions and inputs to automated systems can be clarified. There is an outright responsibility from the engineering community to achieve this.

The case for a system to detect and warn of blockages is therefore compelling, especially if it is a system capable of detecting blockages both in the air and on the ground. However, even a system operable on the ground would be worthwhile, and a starting point for one usable during flight. The goal is to consider the physics basis of a ground operable acoustic reflectometry system, requiring no change to current Pitot tube designs and which may be inserted in the pneumatic connections with little modification.

The paper is organised as follows. A review on past applications of acoustic reflectometry is presented in §II. In this section, alternative options for airspeed measurement are also considered. The acquisition of the Pitot geometries is discussed in §III, along with a description of the steps taken to perform the CT-to-FE analysis. In §IV, two different numerical models are developed to assess the feasibility of the detection method. The corresponding experimental measurements are shown and discussed in §V and §VI respectively. Finally, in §VII, an analytical model is employed to describe the physics behind the frequency response of the total pressure system geometry.

II. Acoustic reflectometry and alternatives to Pitot tubes

Interest in using acoustics for detection of faults dates back many years. Some engineering applications include detection of pipe leakages [12–14], blockages in heat exchangers or sewers [15, 16], non-destructive testing of materials using ultrasound [17] and early warning of blockages in nuclear reactor sub-assemblies [18]. The results from nuclear applications proved the detectability and utility of standing waves, giving good agreement with measurements. Acoustic reflectometry has also shown potential for medical applications. A most impressive success story is in detection of middle ear effusion (liquid in the middle ear). In young children this can lead to hearing problems and speech impairment, and early diagnosis is critical. In 1984, acoustic reflectometry was trialled for fluid detection, and has since become a simple, handheld test routinely deployed with confidence in hospitals [19]. Similar approaches have been applied for detection of airway obstructions in newborns [20].

The aerospace community has shown some interest in acoustic detection for Pitots, as evidenced by a comprehensive IP/patent landscape [21], but primarily there has been a strong historical interest in optical air data systems to remove Pitots entirely and their blockage risks [22–27]. This has come from a desire to measure airspeed, and also from an intention to observe turbulence approaching an aircraft to bring about safety benefits. Tests for the EU NESLIE [28] (NEw Standby Lidar InstrumEnt), DANIELA (Demonstration of ANemometry InstrumEnt based on LAser), AIM (Advanced In-flight Measurement) and AIM2 projects showed that optical systems can measure true airspeed accurately and it appears that this technology may well form the basis for a standard or complementary instrument to the Pitot tube. There are, however, some considerable drawbacks at this stage. At present, no system is commercially available. Replacement of devices on the current fleet would be prohibitively expensive in lost revenue and materials (device is of different size and shape to a Pitot), and a supporting measurement of air density must be made to convert from true airspeed to dynamic pressure (which is the final desired measurement for aircraft manoeuvring). Density measurement is not an obstacle, but might require an external probe, and it would be expected this would be as critical to safe operation as the original Pitot tube it replaced. Optical systems may, however, present the longest term solution for reliable airspeed measurement.

Further work in the aerospace sector has focused on deriving alternative estimates for airspeed using inertial, GPS or flow angle measurements, as successfully demonstrated by Rhudy *et al.* [29]. This is termed 'analytical redundancy' (as opposed to the 'physical redundancy' of multiple probes). This avenue holds great potential for checking the validity of measurements in-flight, but requires a comparison of data sources and is, therefore, not viable before flight (when all systems and Pitots indicate zero speed irrespective of any blockages). It may also require a flight dynamics model of the aircraft, which may contain a modest degree of uncertainty depending on the configuration and conditions for a specific aircraft. Nonetheless, this technique should clearly be pursued.

The acoustic reflectometry approach tested here has been presented in many settings and is subject to a wide range of patents; these are available from a recent UK patent [21] and the associated background patent search. However, the goal of this work is to determine the actual behaviour of a real Pitot when this approach is used; it is this behaviour that has remained unpublished.

It is well known that open and closed tubes exhibit different acoustic behaviour. Once a specific frequency of excitation has been selected, the response (wave reflected from the blocked or open end) may be either larger or smaller in amplitude as a consequence of a blockage (although likely, it is by no means certain the reflected wave amplitude is higher for a blocked case, as this depends on the frequency selected). The premise for the system proposed here, and elsewhere, is therefore to transmit a known frequency down the Pitot using a speaker and measure the excitation level some short distance away from the speaker (Fig. 1(b)).

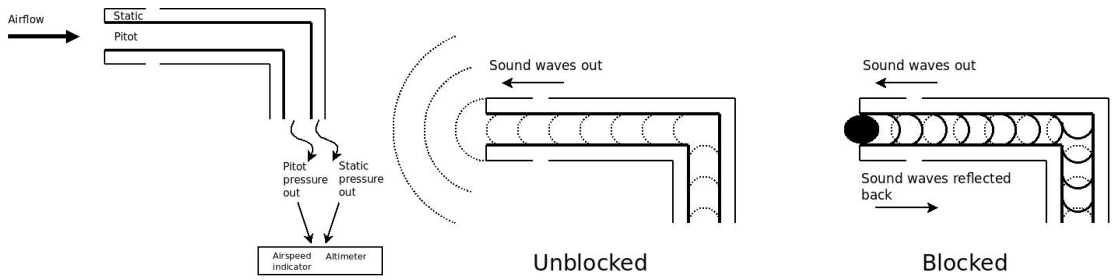

(a) Schematic of Pitot-static tube (b) Acoustic reflectometry approach

Fig. 1 : Pitot-static operation and acoustic blockage detection.

There is a significant gulf between such a basic principle of operation and a workable device. The complicated internal shape of the Pitot affects the response and blockages can consist of insects, nests, ice or tape. The acoustics of each will be different, but must be measured to have confidence in the system. This is the target of the work presented here. To have the strongest dataset, both numerical and experimental results need to provide evidence to support the feasibility of detection.

III. Geometry acquisition

Three Pitot-static tubes from a 737 (-300/-400/-500 series) and three from a 747 (-400 series) were acquired from an aircraft breakers yard. Although not suitable for resale use due to limited further life, these tubes were otherwise in flight condition and came from aircraft that made their final flight directly to the breakers yard, with their Pitots operational. The 737 and 747 devices are of notably different size due to the influence of fuselage size on measurement accuracy (Fig. 2). Each tube has a single Pitot head and two static ports, as well as drain holes for releasing moisture. The

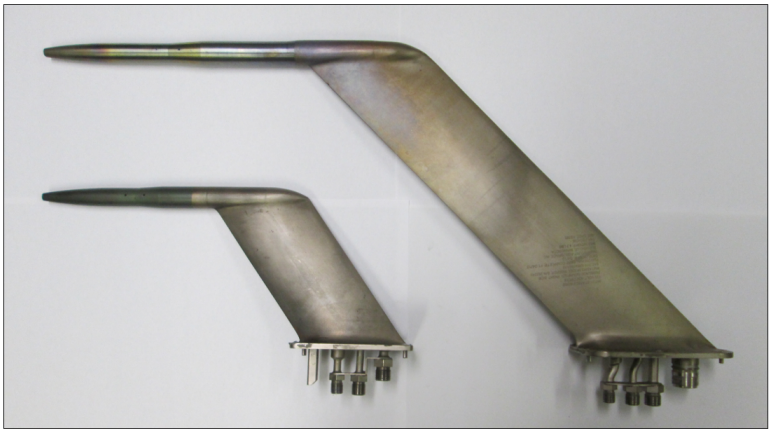

Fig. 2 : 737 and 747 Pitot-static tubes.

goal of the three-dimensional finite element study was to provide an accurate model to understand the fundamental effects of Pitot head blockages on the total pressure system frequency response to acoustic excitation. In order to ensure this goal was met, the internal structure of the Pitot-static tube was captured using x-ray computed micro-tomography, or micro-CT (Fig. 3). The platform

used was the Nikon XTH225ST based at the National Composites Centre (NCC) in Bristol. It has 5-axis manipulation capability and 3-micron focal spot size, with a maximum beam energy of 225 kV. Due to the maximum sample size being 300 mm × 300 mm, two lengthwise scans had to be performed for the 737 Pitot in order to capture the whole geometry. For each scan, a 200 kV, 9.9 W micro focus x-ray source was used with an exposure time of 2 seconds-per-projection to ensure penetration through the Pitot tube. Reconstruction of the captured radiographs was performed using Nikon proprietary software CT-Pro 3D. The three-dimensional volume produced was viewed and analysed to extract the necessary dimensions using Volume Graphics VG Studio MAX software. A model based on extracted two-dimensional images, taken from the three-dimensional volume, was constructed using ImageJ [30] to extract the data points from the two-dimensional cross-sections, translating the selected voxel sizes to dimensions that could be imported into CAD. ImageJ was also used to obtain the centreline for the tube curvature in order to accurately loft between cross sections.

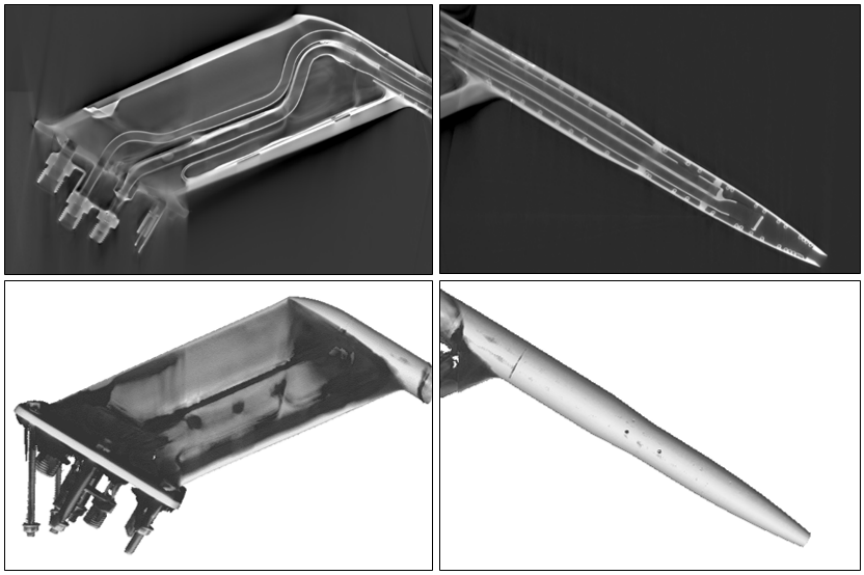

Fig. 3 : CT scans of 737 Pitot-static tube 1.

The 737 Pitot tube is seen to consist of three pressure systems, one for total and two for static pressure readings, as shown in figures 3, 4 and 5. The helical heating element (repeated grey circles along periphery of Pitot in figure 4(a)) is present around the inner circumference of the cylindrical section of the Pitot; it is not used in the support strut section. The total pressure system (T) has a baffle plate integrated into the tube (Fig. 6). Two slits (figure 5) are used to measure the pressure, while the baffle plate is designed to keep water and other debris from entering the Pitot head.

The static pressure system 1 (S1) begins behind the Pitot head. The S1 tube is connected to a static air chamber, enclosed by boundaries (a) and (b) within which there is a small gap in the tube (Fig. 4(a)). The holes located in the circumference of this region ensure that static pressure is being measured. After boundary (b), the Pitot tube has two bounded tubes as well as the air around

them, which is now enclosed by the outer casing. In this region, another set of static pressure holes is present, making the resultant domain inside it the second static pressure system (S2). Having dual static ports helps remove static pressure errors due the aircraft pressure field, as well as pitch and yaw [31].

Drain holes are present throughout the pressure head to remove moisture from the interior. The most pertinent features for the acoustic behaviour are the baffle end and the shape of its covering chamber, as these strongly influence how acoustic waves will reflect both with and without a blockage located at the Pitot head entrance.

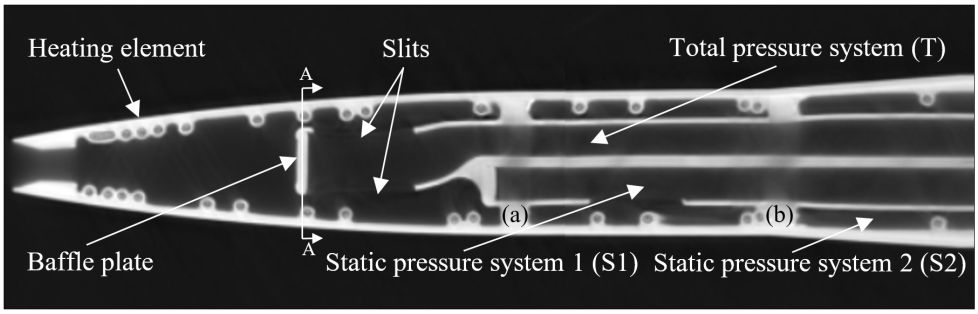

(a) micro-CT scan (section A-A labelled)

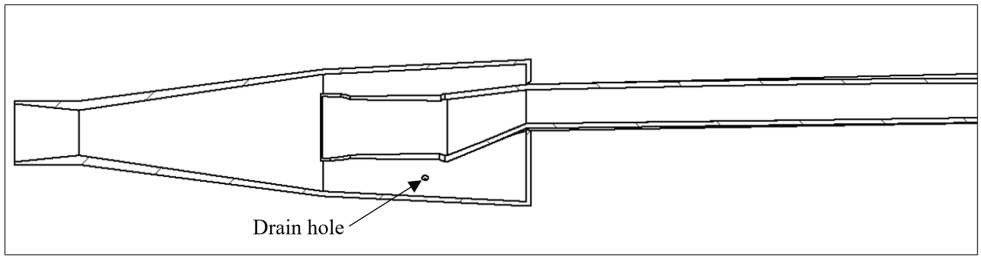

(b) CAD for total pressure system Pitot head

Fig. 4 : 737 Pitot-head cross-section.

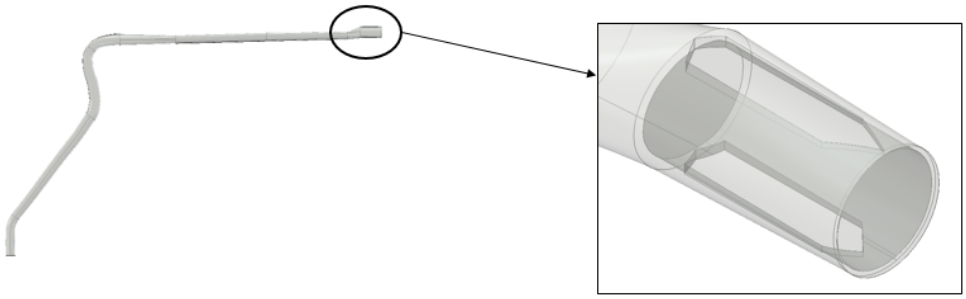

Fig. 5 : CAD modelling of slit design in 737 Pitot tube.

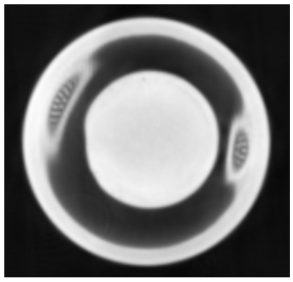

Fig. 6 : Section A-A — baffle plate section view into the Pitot (Fig. 4(a)).

To understand the geometry of the 747 Pitot tube, an X-ray scan was also performed. This showed that the pressure systems are ducted differently to those in the 737 scans, although the overall configuration of the Pitot head itself is very similar. For the 747 tube, both static pressure systems are ducted and are blocked at the end. They do not have the slit configuration seen in the 737 tube. The total pressure system is connected to the chamber of the Pitot, as illustrated in figure 7. A bundle of heating wire is fixed near the upper edge of the strut chamber.

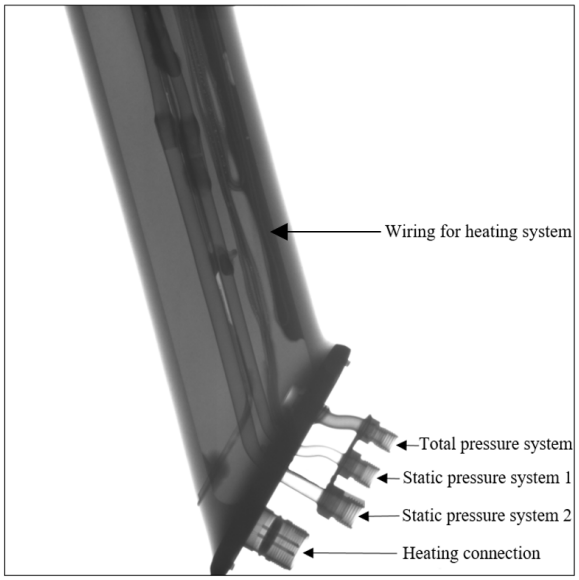

Fig. 7 : X-ray scan of 747 Pitot-static tube root region.

IV. Numerical study

Two finite element studies were performed using the commercial software COMSOL Multiphysics®; the first was based on a simple straight tube, while the second addressed the full total pressure system of a 737 Pitot. A pressure acoustics, frequency domain interface was employed within COMSOL as it permits modelling acoustics phenomena that do not involve fluid flow. In both studies, the domains were filled with air at standard conditions.

Formulation

The time-harmonic formulation applied within COMSOL [32] uses the Helmholtz equation:

$$\nabla \cdot \left(\frac{\nabla p}{\rho} \right) + \frac{\omega^2 p}{\rho c^2} = 0 \tag{1}$$

where c is the speed of sound, p is the pressure, ρ is the density and w is the angular frequency. Sources here are applied through the boundary conditions.

The steady-state frequency response was computed with a parametric sweep over a frequency range (10 Hz to 3000 Hz) using a harmonic load. Equation 1 was solved for the complex pressure, $p(x, y, z)$, which can be translated into sound pressure level, SPL, in post-processing:

$$p_{rms}(x, y, z) = \frac{1}{\sqrt{2}} |p(x, y, z)| \tag{2}$$

$$SPL(x, y, z) = 20 log_{10} \left(\frac{p_{rms}(x, y, z)}{p_{ref}} \right) \tag{3}$$

SPL is frequently used in acoustics and is a logarithmic measure of the effective pressure of sound relative to a reference value, p_{ref}. The reference pressure is 20 µPa, which is the threshold of human hearing (i.e. 1 Pa is equivalent to an SPL of 94 dB). The SPL results were normalised when comparing numerical and experimental studies since the experimental input boundary condition at the Pitot insert was unknown. Normalisation was done by dividing the respective dataset by its maximum value:

$$\hat{SPL}(x, y, z) = \frac{SPL(x, y, z)}{SPL_{max}(x, y, z)} \tag{4}$$

where the normalised SPL data is given by $\hat{SPL}$.

Study 1: Two-dimensional axisymmetric straight tube

A first analysis was performed on a hollow acrylic tube for which experimental data was available. This was conducted so that any subsequent differences between a Pitot and a plain tube could be shown clearly, to test the numerical modelling setup on a more basic case and also to observe the influence of partial rather than complete blockages. Analysis consisted of a frequency sweep from 10 Hz to 3000 Hz using 5 Hz steps, with a simple radiation condition used for modelling the far-field as an infinite space, using a straight tube 496 mm long with a 23 mm inner diameter (Fig. 8(a)). A triangular mesh was used with maximum edge length, h_{max}, being constrained by:

$$h_{max} = \frac{c}{ppw \times f_{max}} \tag{5}$$

where the acoustic speed, $c = 343$ m/s, and the maximum frequency, $f_{max} = 3000$ Hz. Although literature advises 6 to 10 nodes per wavelength [33], 12 points-per-wavelength, ppw, were employed in equation 5 to ensure the quality of the results would not be compromised. This yields a maximum edge length, $h_{max} \approx 0.00953$ m.

The mesh consisted of 2340 domain and 206 boundary elements (Fig. 8(b)). Due to the axisymmetric nature of the study, a semi-circle of radius 0.2 m was used to model the far field domain for the unblocked condition (Fig. 8). For all cases, a plane wave radiation boundary condition of incident pressure amplitude, $p = 1$ Pa, was applied at boundary 1. Furthermore, a sound hard boundary condition was applied at boundary 2. For the blocked condition, the far-field was neglected and boundary 3 was also made sound hard. For the unblocked condition, boundary 3 was left open, with the far field boundary 4 being defined by a spherical wave radiation condition with its source located at z = 0.496 m (centre of the tube at the unblocked end). This radiation condition sets a boundary that will not reflect normally incident plane or spherical waves.

(a) Geometry (b) Mesh

Fig. 8 : Two-dimensional axisymmetric numerical study for straight tube.

For the progressive blockage parametric study, a blockage model was added to the end of the tube. The blockage started from the inner radius with a length of 0.1 mm, increasing to 23 mm in the direction of the tube centre. In order to obtain high data resolution for the frequency response, 70 equally sized steps were used between the minimum and maximum length values. Since the study was axisymmetric, at length = 23 mm, the blockage fully covered the tube cross section, modelling the fully blocked condition. Blockage boundaries were modelled as sound hard surfaces. Numerical results were extracted at a location 10 mm from the entry point of the plane wave to match the measurement point for the experimental results.

Figures 9 and 10 show that the experimental and numerical results are in good agreement for both unblocked and blocked cases. The position of the minima/maxima is dependent on the boundary condition at both ends of the tube. The inlet has a plane wave condition, while the outlet changes from Neumann to Dirichlet, yielding a phase shift. A blockage produces a shift of the first minima in the response spectrum from 350 Hz to 180 Hz (170 Hz difference). This is substantial, making detection of blockages for a straight tube simple. Deviations from the experimental results are most likely attributable to interactions with the structure of the open tube, or the detailed shape of the speaker and inlet cone, which were not modelled (as a plane wave at the inlet was assumed).

Figure 11 for progressive blockage shows the suitability of this model for the later analysis in §VI. Although changes in $S\hat{P}L$ peak response location appear quite small with changes in fractional

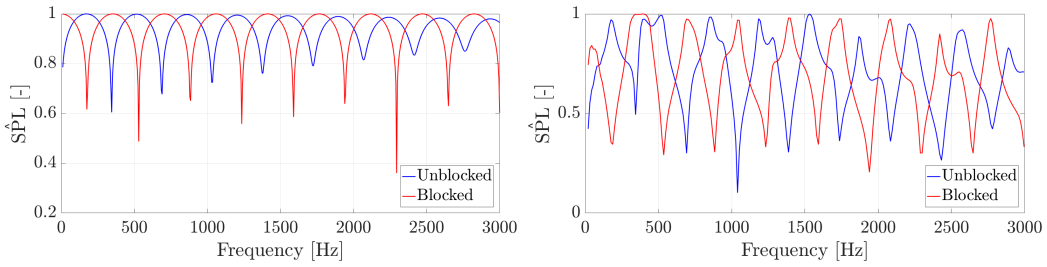

(a) Numerical (b) Experimental

Fig. 9 : Straight tube — blocked vs. unblocked results for numerical and experimental studies.

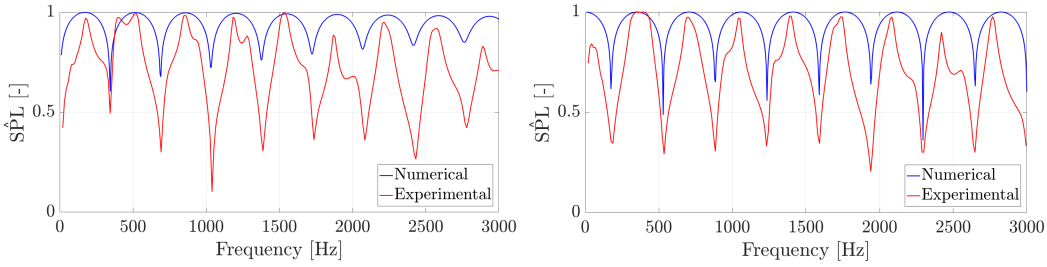

(a) Unblocked case (b) Blocked case

Fig. 10 : Numerical vs. experimental tests for straight tube.

blockage, these correspond to large and easily detectable changes because the troughs themselves are very sharp. A notable trend is visible in figure 11: blockage detection is frequency dependent. The effect of the dual boundary condition (Neumann and Dirichlet) at the exit is clearer at low frequencies, for very high area blockages. This implies the lower frequencies are the most suitable part of the spectrum for blockage detection. Nevertheless, figures 10 and 11 show that there remains a change at all the frequencies that were investigated.

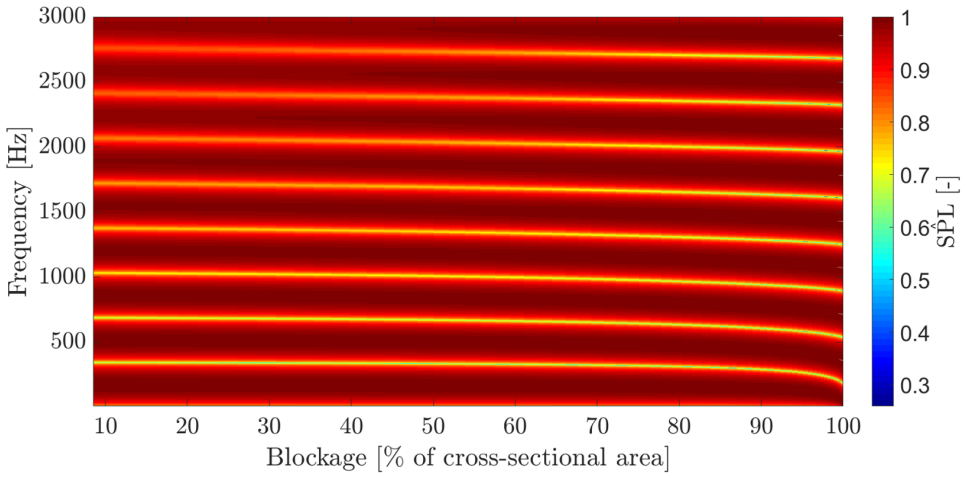

Fig. 11 : Progressive blockage study.

Study 2: Three-dimensional 737 Pitot-static tube

Since the different pressure systems (T-total, S1-static 1 and S2-static 2) are independent of each other, any acoustic analysis can be performed for each separately. Based on overall accident reports, priority here was given to the Pitot head; indeed for icing it may be observed that the majority of accretion occurs here as this is the location with the highest water catch [34]. The excitation frequency sweep again ranged from 10 Hz to 3000 Hz using 5 Hz steps.

For the blocked condition, sound hard and interior sound hard boundary conditions were employed where appropriate. A plane wave boundary condition with an incident pressure amplitude of 1 Pa was applied at the base of the pressure system. This simplification means that potential acoustic disturbances caused by the cone, porous media and connecting tube were not modelled (see §V). Furthermore, the two drain holes were modelled using an air impedance boundary condition to model the acoustic waves leaking out of the system.

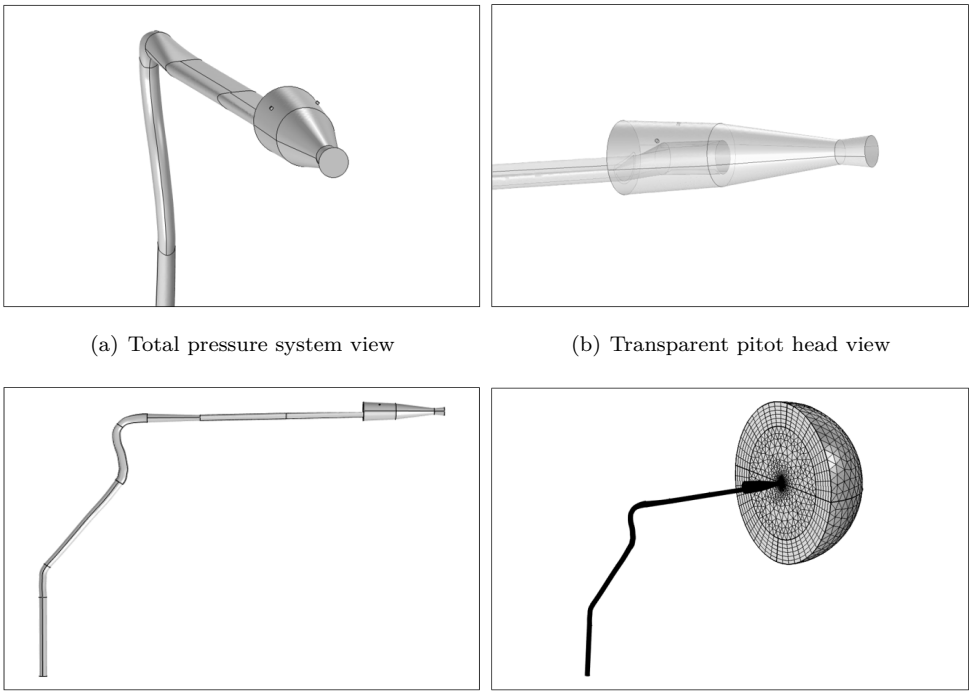

(a) Total pressure system view

(b) Transparent pitot head view

(c) Total pressure system geometry

(d) Unblocked geometry and Perfectly Matched Layer (PML) mesh

Fig. 12 : Blocked and unblocked 737 Pitot CAD geometries.

The far-field for the unblocked case was modelled through the use of a perfectly matched layer (PML) [35] for highest accuracy. The PML developed is characterised by two layers of meshes and was designed as a semi-sphere due to the direction of the waves leaving the Pitot head when unblocked. The inner layer is tetrahedral while the outer layer is swept using quadrilateral elements for all of the five sub-layer elements (Fig. 12). Although the PML is ideally designed to be non-reflecting, some reflection may occur due to numerical discretization. The PML was kept some

distance from the Pitot head such that this effect was minimised. A conservative approach was taken with regards to the sizes of each layer to ensure enough space was provided to model infinite space accurately, despite the additional computational time required. The inner and outer layer semi-spheres had an outer radius of 0.085 m and 0.1 m respectively.

A tetrahedral mesh was used for the total pressure system geometry (Fig. 12), where the maximum edge length, h_{max}, was the same as in §IV-Study 1 since the constraints applied through Eq. 5 were valid here. For tetrahedral elements, the element area ratio, q, is evaluated using:

$$q = \frac{72\sqrt{3}V}{(h_1^2 + h_2^2 + h_3^2 + h_4^2 + h_5^2 + h_6^2)^{3/2}} \tag{6}$$

where V is the element volume, and h the respective edge lengths [36]. The meshes generated yielded average element qualities of 0.7402 and 0.7415 for the blocked and unblocked cases respectively, where a maximum value would be 1 (Table 1, Appendix A). These were found to give an adequate balance of the number of elements and their quality, while also ensuring a satisfactory resolution of the geometry modelled.

Figure 13 shows results obtained from the three-dimensional finite element model of the Pitot-static total pressure system, for the blocked and unblocked conditions. Measurements were taken at the same location as the microphone in the experiments in §V. The biggest difference between blocked/unblocked conditions occurs at the lower frequency range, from 10 Hz to 1200 Hz. This difference dissipates with increasing frequency, a trend that was not evidenced in the straight tube model in figures 9 and 10, and which must therefore be linked to the geometry of a real Pitot.

Due to the existence of two slits followed by a baffle plate in the total pressure system, it was critical to ensure that the acoustic waves would go through the slits. If the waves were to reflect straight off the baffle plate, it would be very difficult to discern a blockage at the main entry to the Pitot head chamber. Figure 13 shows that sound waves in the studied frequency range pass through the slits, otherwise, there would be no differences between the unblocked and blocked results. The coalescence of the blocked and unblocked responses is discussed in §VII.

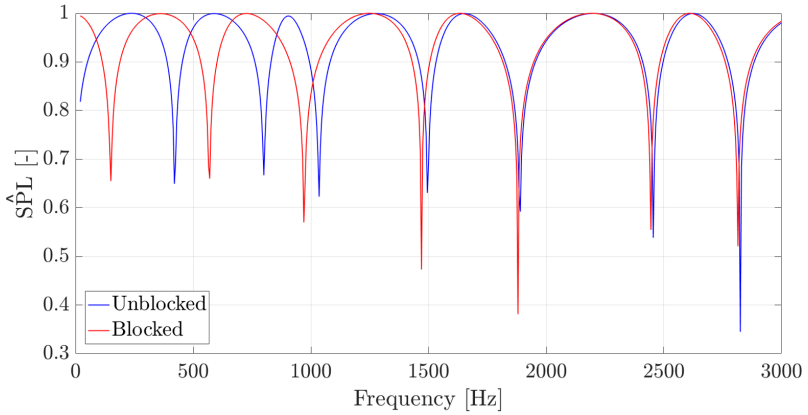

Fig. 13 : Three-dimensional numerical study – total pressure system for 737 Pitot-static tube.

V. Experimental study

Tests were conducted in a 8×4.5×5 m pyramidal-cone anechoic chamber to limit reflections which could contaminate the measurements. The chamber had a cut-off frequency of 570 Hz. Experiments were carried out with the unblocked case and with various blockages. Four types of blockages were analysed and compared to the unblocked case. These were tape, foam, pre-deceased insects (*Bombus Terrestris*) and metal (steel), where foam and steel were studied as representatives of soft and hard ice respectively (Fig. 14). To minimise reflections into the test article when running the unblocked test, the setup was positioned in the middle of the chamber, with the Pitot tube exit pointed to the top corner of chamber which was the furthest point from the setup (Fig. 15).

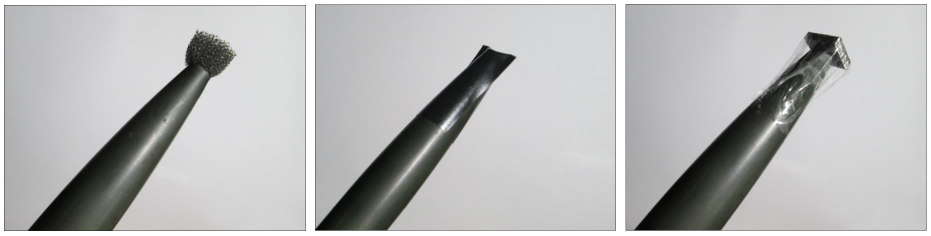

(a) Foam (b) Tape (c) Metal (Steel)

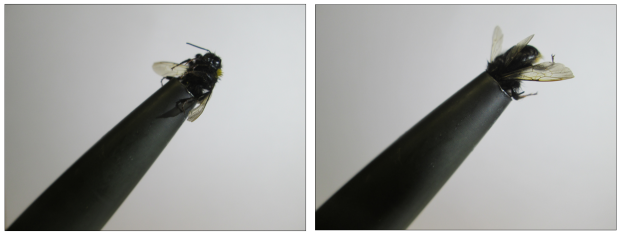

(d) *Bombus Terrestris* (abdomen first) (e) *Bombus Terrestris* (head first)

Fig. 14 : Illustration of different blockage types.

Experimental setup and basic methodology

A sweep of sine waves of frequencies up to 3 kHz was generated by the Tektronix AFG3021C signal generator and played using the Visaton FR10-HM 8 Ohm speaker [37]. Given the less reliable behaviour of the speaker at lower frequencies (below ∼150 Hz), data in this region is not interpretable, but falls below the region of interest (Appendix B). The speaker was attached to a contracting cone which was filled with 20 ppi (pores per inch) foam. This damps out standing waves within the cone and filters out higher acoustic modes, while also ensuring the plane wave mode amplitude is not attenuated. The effect of the cone was to only allow for the propagation of plane waves into the Pitot.

Two different aluminium tubes were designed and manufactured to connect the end of the cone to the Pitot tube total (T) and first static system (S1) pressure ports due to difference in diameters (threads are different for all pressure lines, most likely to make incorrect connection impossible).

The FG-23329-P07 analog omnidirectional electret condenser microphone was used to capture the pressure in the duct and relay this as an electrical signal (i.e. voltage). This was then converted to pressure units by knowing the microphone sensitivity, which was obtained via calibration before testing (Appendix C). The pressure measurements were used to compare the blocked and unblocked conditions to evaluate the feasibility of developing a detection method. A microphone holder was 3D printed and fitted around the tube such that the microphone was perfectly flush-mounted (16(a)). The microphone has a circular sensing area of 0.8 mm, hence a 0.4 mm hole was drilled in both the microphone holder and aluminium tube to avoid expansions and contractions, and to reduce dispersion errors. The hole was approximately 10 mm from the exit of the Pitot tube insert. Silicone sealant was used to ensure the two holes aligned properly before testing to prevent acoustic leakages between the tube and microphone holder. Thread seal tape was utilised to fix the tube to the cone (Fig. 16(b)).

Fig. 15 : The Pitot tubes were placed in the centre of the chamber — by using a 3D printed Pitot tube mount, the Pitots were pointed towards the top corner of the anechoic chamber to minimise reflections back into the system.

The data captured was processed using the NI USB-9215A DAQ system with the NI USB-9162 C Series USB Single Module Carrier. Each excitation frequency was measured for 2 s at a sampling frequency of 42,000 Hz. This means the range of frequencies considered here could easily be captured. In post-processing, the mean system noise was then subtracted, the power spectral density of the signal analysed and the sound pressure level, SPL, computed.

Input voltage study

The FG-23329-P07 microphone clips if the signal is > 124 dB [38] so, for both Pitot tubes tested, a sweep of signal generator input voltages was performed (Fig. 17). This investigation allowed for the selection of an input voltage for each Pitot tube to avoid clipping in the measurements and to ensure the sound pressure level was high enough to produce clear results. Figure 17(a) shows that

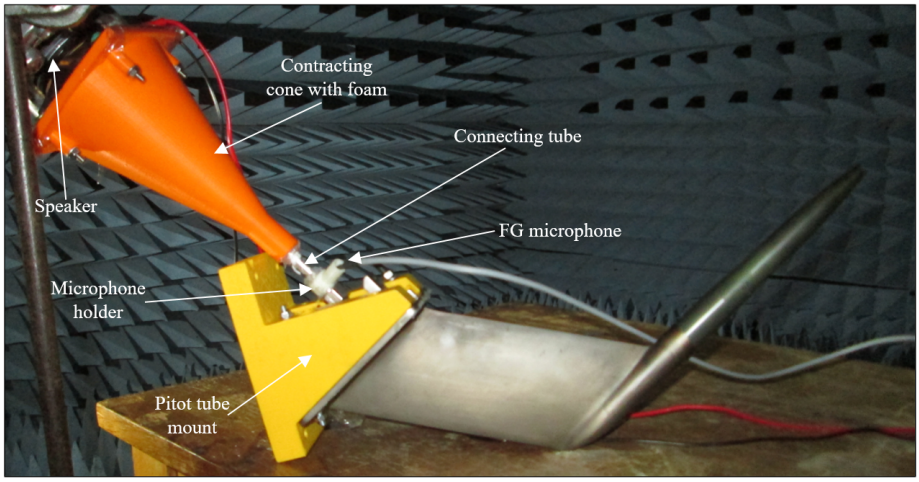

(a) Close-up of setup: the sound source (speaker) was connected to the contracting cone to damp out standing waves. The plane wave then travelled along the connecting aluminium tube and into the Pitot insert. The pressure was recorded using an FG-23329-P07 microphone which was securely fastened using a 3D printed holder.

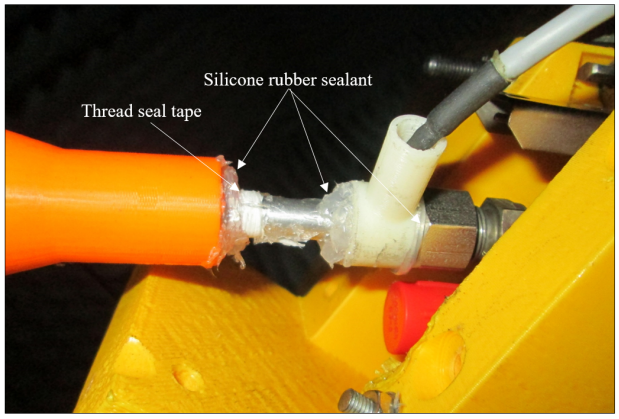

(b) Close-up of connections: leakages were minimised by using silicone rubber sealant and thread seal tape at the joints.

Fig. 16 : Experimental setup.

as the voltage is lowered, the response curve converges to a fixed shape (although the magnitude of the response of course continues to drop), while the response for the 747 tube in figure 17(b) is quite consistent over the full range tested. From the results shown, 0.25 V was selected for the 737 Pitot tube. Due to the difference in length when compared to the 737, a voltage study was also undertaken for the 747 Pitot tube, and a voltage of 0.10 V was selected (for the static line measurements, the 737 and 747 tubes again used 0.25 V and 0.10 V respectively).

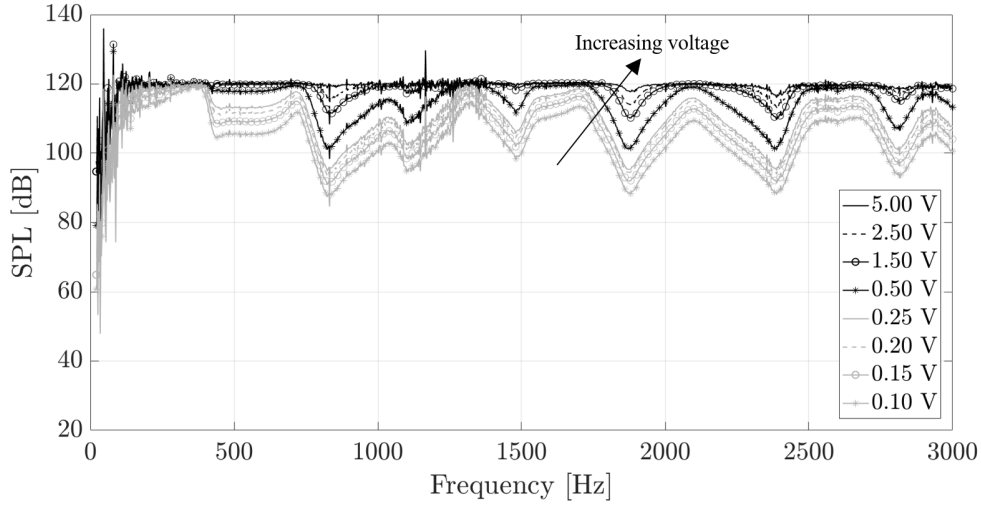

(a) 737 Pitot input voltage study

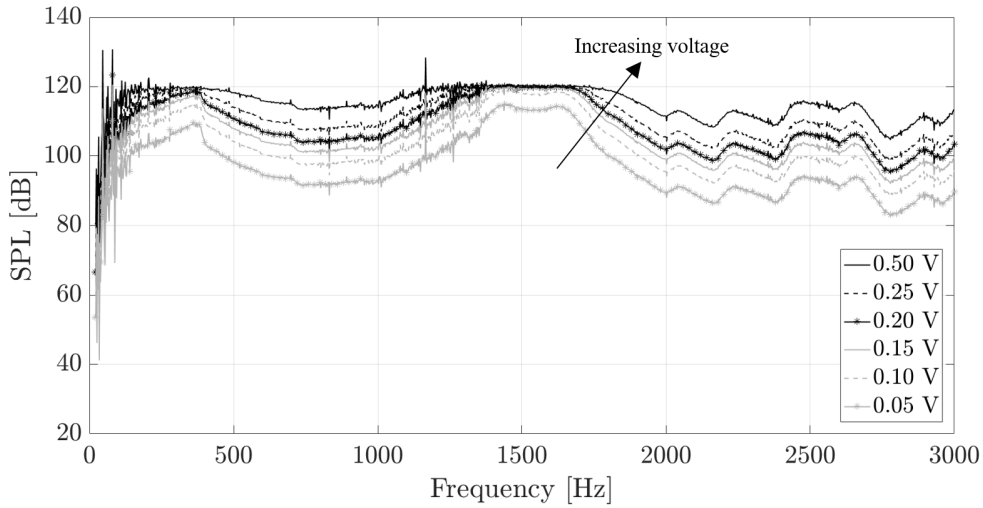

(b) 747 Pitot input voltage study

Fig. 17 : 737/747 experimental input voltage studies.

VI. Implications for practical blockage detection

Total pressure system

Before any blockage detection system may be proposed, it is of fundamental importance to understand any variation between between Pitots of nominally the same design (ie. to quantify any variations in manufacturing or arising from wear), so this was explored for the total pressure line for the 737 design in figure 18(a) and for the 747 design in figure 18(b). Figure 18(a) shows very similar behaviour between 737 tubes 1 and 2, but tube 3 has a slight difference. Exploration revealed that a drain hole on the tube was blocked, most likely from corrosion, and it is believed this altered the response as seen here. The 747 results in figure 18(b) also show some slight variation between tubes, but in addition to partially obstructed drain holes (no fully blocked drain hole was found but partial blockages may have remained), this may also have been caused by a different internal

configuration. The use of a heating wire bundle in the strut of the 747 design (Fig. 7) means some acoustic variation is to be expected. The conclusion from these results is that acoustic behaviour is generally consistent between Pitots, however a much larger sample size would need to be tested to confirm this for manufacturing/calibration purposes. Drain hole blockages could conceivably cause an acoustic system to detect a blockage where none existed. Whether this is desirable is uncertain; one could equally well argue a drain blockage should be investigated before flight, or that it might be a crew annoyance. The 747 data in figure 18(b) does however support designing Pitots to avoid any variability in manufacturing, because if reflectometry is to perform well the pressure lines need to function as acoustic waveguides, and any irregular objects (such as wire bundles) impair this. Similarly, transmitting the pressure via any chamber which is not of constant sectional area will interfere with the acoustic behaviour.

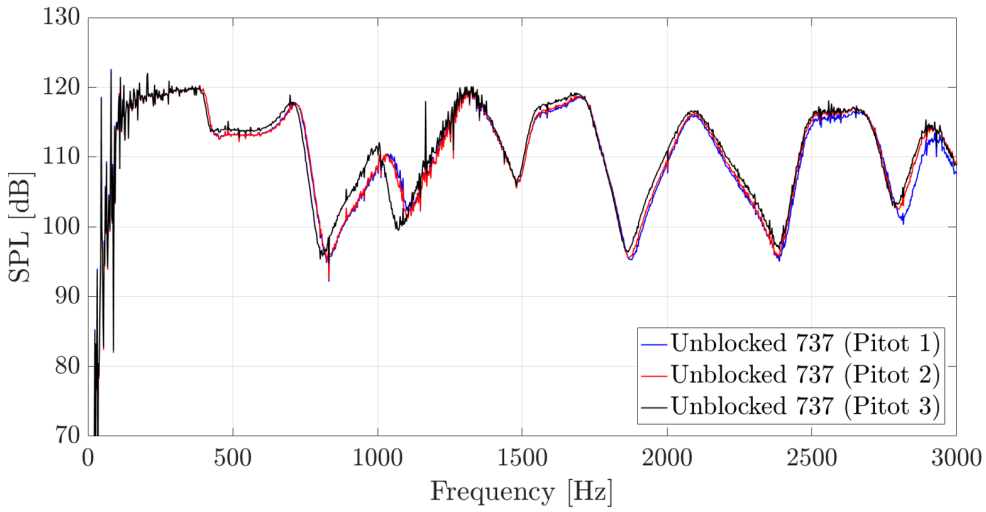

(a) 737 Pitot head, tubes 1, 2 and 3, unblocked

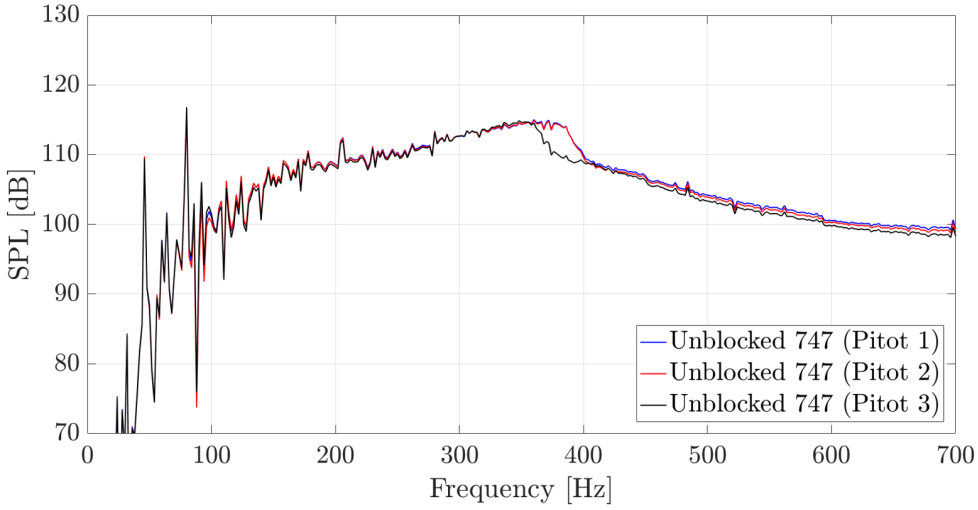

(b) 747 Pitot head, tubes 1, 2 and 3, unblocked

Fig. 18 : Comparison of 737 and 747 unblocked Pitot head acoustic responses between different tubes.

The most critical results are shown in figures 19 for the 737 tube. A clear difference in SPL is visible between blocked and unblocked conditions from 600 Hz to 1050 Hz, repeated between the three tubes and all blockages, with a variation ranging from 10 dB to 15 dB. The convergence of the unblocked and blocked results at higher frequencies (Figs. 13, 19 and 20), attributable to the complex baffle and slit design employed in the Pitot head, was observed both experimentally and numerically, and appears to preclude use of higher frequencies for detection. This will be considered in more detail in §VII. Steel, tape, foam and insect blockages were all detectable. Zooms of these results are given in figure 20 and it seems clear that, from a physics point of view, a workable device could be built to use frequencies ranging between 600 Hz and 1050 Hz.

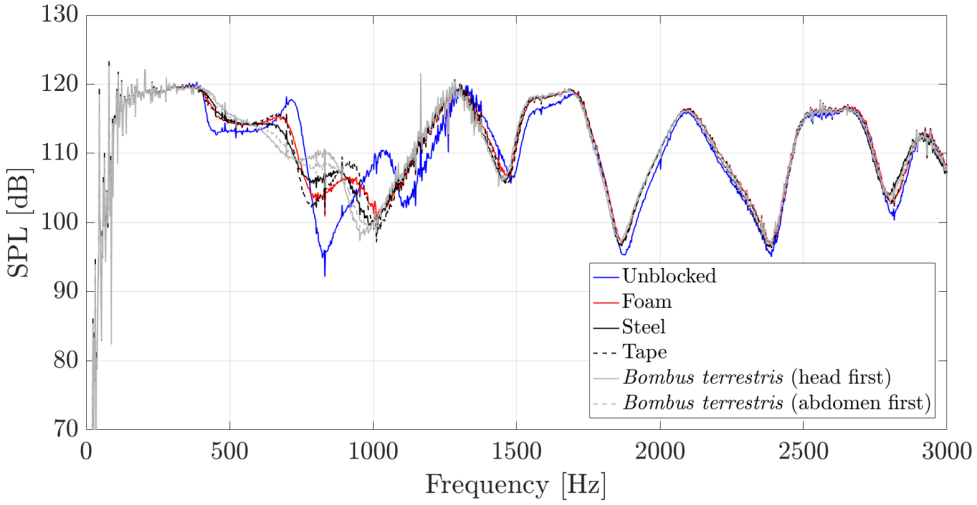

Fig. 19 : 737 Pitot head experimental results, tube 1, unblocked vs. blocked.

The point at which a blockage would be detected is clearly important. A study of how progressive blockage affects the acoustic response of the total pressure port was undertaken with the 737 Pitot 1 (Fig. 21). Four tests were performed using adhesive tape where 25%, 50%, 75% and 100% of the head diameter were covered. As shown in figure 21, blockage starts to be clearly detected at between 25% and 50%. Unfortunately, there can be no reliable correspondence between the blocked fraction and the error that this produces in the airspeed reading. Depending on the blockage shape, what is assumed to be total pressure becomes (through introduction of the blockage) a static pressure at an unknown point around a body of arbitrary shape. This is obvious if a particularly nefarious situation is envisaged, whereby the Pitot head is entirely unblocked, but an object is placed close to the entrance such that the flow is altered (this could even be a flat plate upstream). The total pressure will no longer be measured and the system will be in error. This would never happen in practice, but it illustrates that a more sensitive detection system is preferable.

Figure 22 shows that the 3D numerical study demonstrates good agreement with experiments above both the transient frequencies at which the speaker is unable to produce clean sound waves

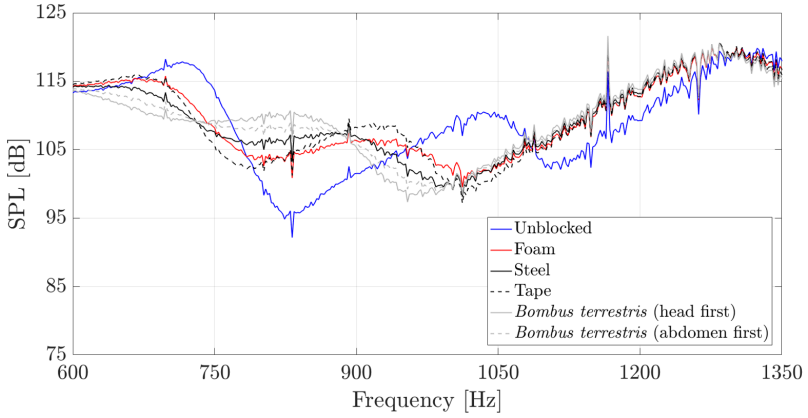

(a) Tube 1

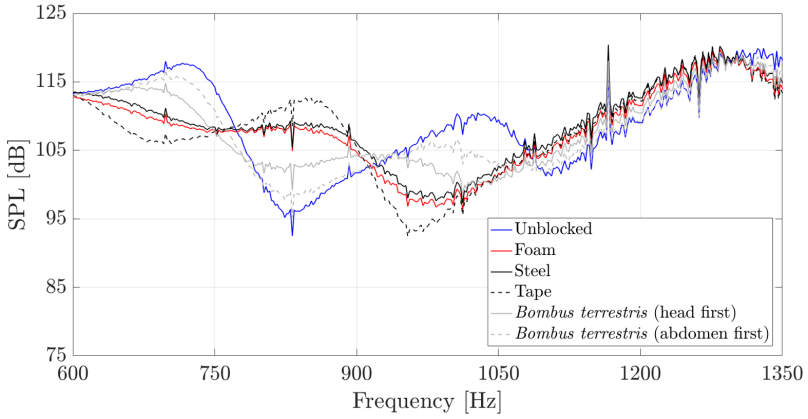

(b) Tube 2

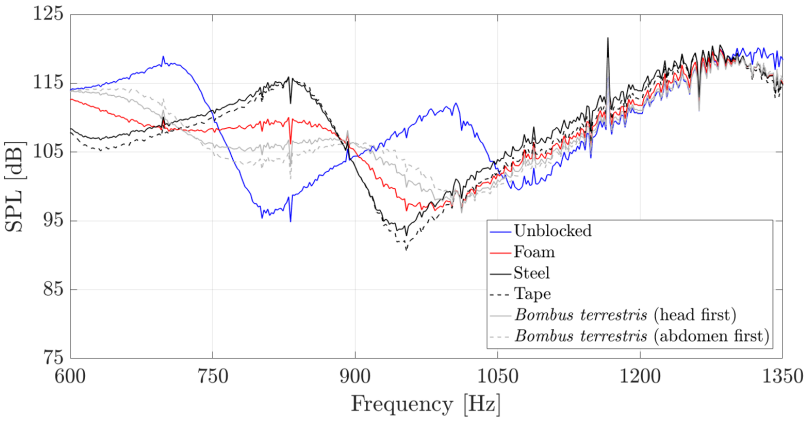

(c) Tube 3

Fig. 20 : 737 Pitot head experimental results, tube 1, unblocked vs. blocked (zoomed).

(400 Hz), and the anechoic chamber cut-off frequency (570 Hz). For the blockage case, figure 22(a) shows that the numerical model best agrees with the *Bombus terrestris* (head first) case at around 1000 Hz, capturing the antinodes accurately from this point onwards. Below this frequency, the numerical model is not accurate for the blocked case. Figure 22 shows that most antinodes in the experiment are captured.

Despite figure 13 demonstrating a difference in acoustic response between the blocked and unblocked cases, the intricacies seen in the experiments between 600 Hz and 1100 Hz are not seen in the numerical models developed. This may be attributed to the speaker amplitude and impedance variation with frequency, cone geometry, acoustic properties of the porous media, the connecting tube or the flush-mounted microphone setup and vibration of the Pitot. All this was simplified to a simple planar wave (of constant amplitude of 1 Pa for all frequencies scanned) which was input at the Pitot tube insert location.

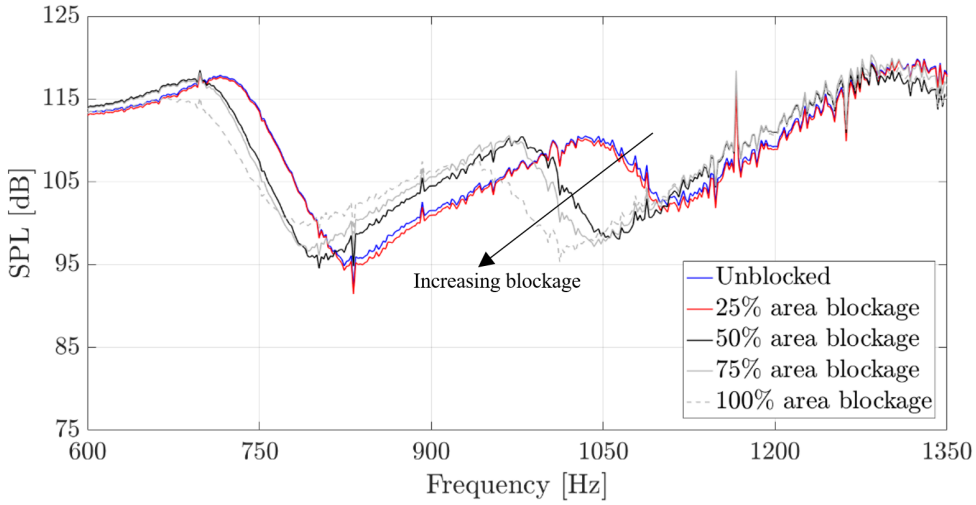

Fig. 21 : 737 Pitot head experimental results, tube 1, progressive blockage study.

Further features of the the experiment not modelled in the numerical study included attenuation and dispersion losses [39]. In reality, the sound wave energy is continuously reduced by these dissipative processes. Attenuation and dispersion effects due to viscosity and thermal conduction are frequently seen when acoustic waves travel inside thin pipes. Thermoviscous effects are especially significant when the representative cross-sectional dimension is much smaller than the vorticity and entropy boundary layer thicknesses [40, 41]. As such, the fact that the simulations do not perfectly match the experimental results is not unexpected.

Figures 23(a) and 23(b) depict the results for the 747 Pitot head. The differences are so small as to be impractical for detection. This is because the 747 total pressure port is not ducted (Fig. 7), unlike in the 737 tube (Fig. 3), and therefore does not act as an effective acoustic waveguide. From this, it may be concluded that ports which are not ducted should not be used for acoustic reflectometry.

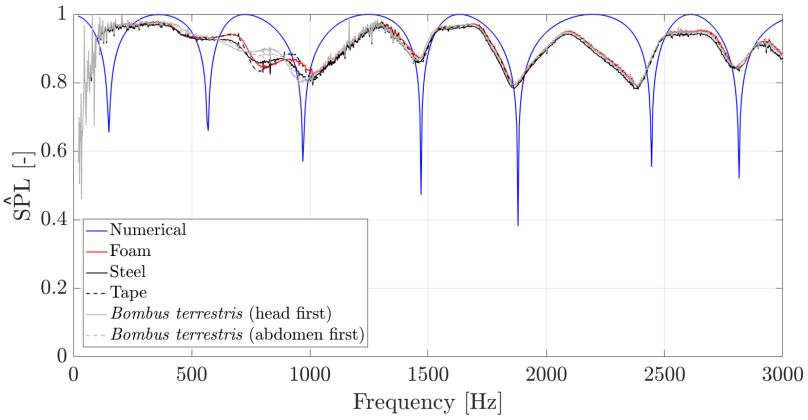

(a) Blocked results from numerical analysis and experimental measurements

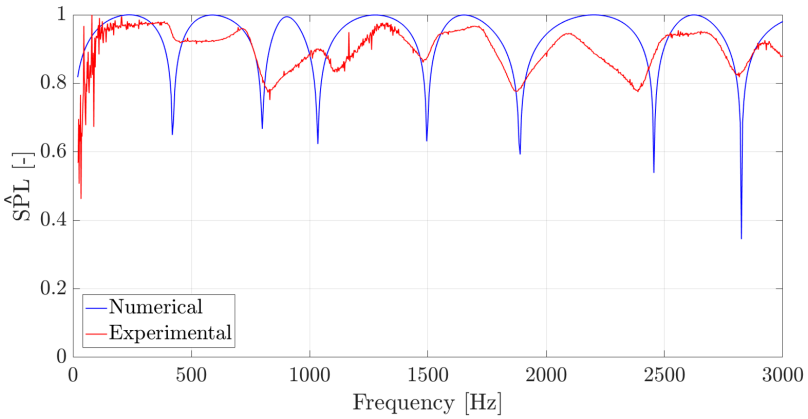

(b) Unblocked results from numerical analysis and experimental measurements

Fig. 22 : Numerical study vs. experimental results for 737 Pitot, tube 1.

Static pressure system

Subsequent testing focussed on the static pressure lines, where the small static ports were blocked using tape. For the 737 Pitot one of the static pressure lines follows a cylindrical duct, while the other is not ducted. The ducted static line was used for the tests performed here. In comparison, both static lines in the 747 design are ducted (evidently because only 1 line is not ducted, and this has already been used for the Pitot head (total pressure line)). Figures 24 and 25 check for consistency within the static lines of the Pitots tested here. Agreement appears good, which would be expected (providing the static holes are not obstructed). Similar behaviour was seen for both the 737 and 747 static lines.

Figure 26 shows the 737 and 747 unblocked/blocked results where blockage was achieved by taping over the ports. For both designs there are appreciable differences over much of the tested frequency range, specifically from 300 Hz to 2300 Hz. It is probable that a system could be designed for operation on the ground (i.e. in a quiet environment) to detect static port blockages. The 737 static line (which was not ducted) was not tested given the poorer results on the 747 Pitot head, and it is likely that an acoustic method would be unsuitable for this configuration.

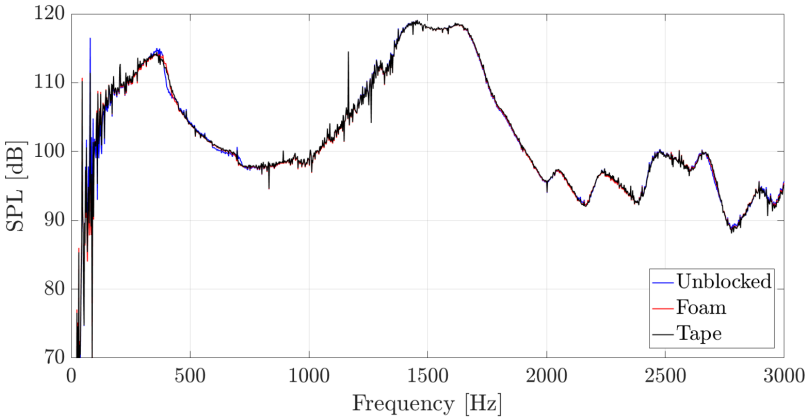

(a) Unblocked vs. tape and foam blockages: full frequency sweep

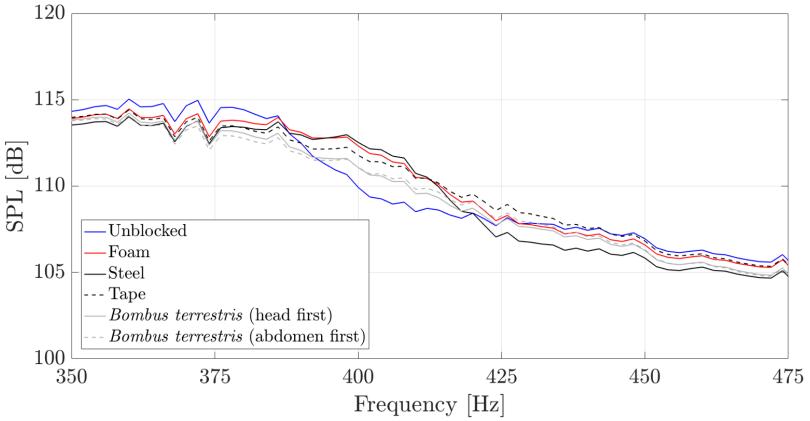

(b) Zoomed

Fig. 23 : 747 Pitot head experimental results, tube 1, unblocked vs. blocked.

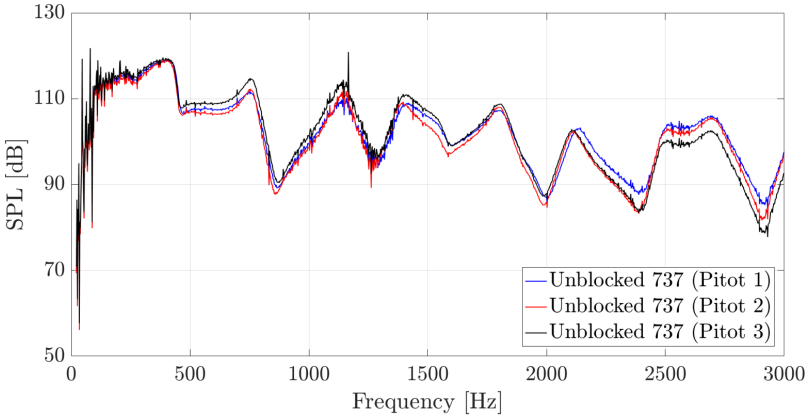

Fig. 24 : Static port experimental results for the 737 Pitot tubes (unblocked).

Overall, it is perhaps surprising that the acoustic approach detects blocked static ports so effectively, given that the ports are only 1-2 mm in diameter, and that they reside in large closed chambers within the probe.

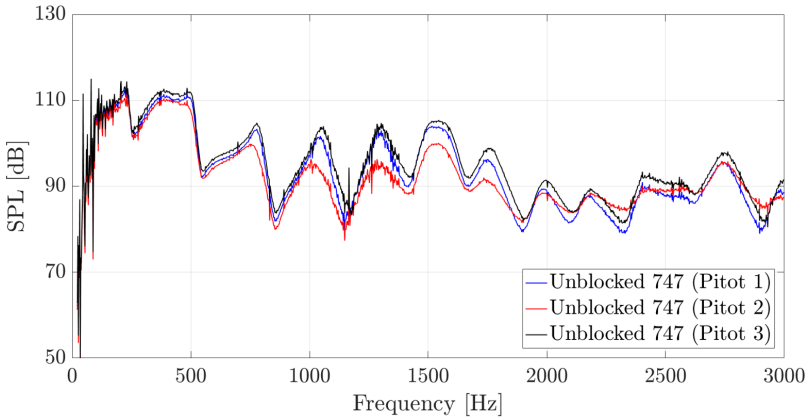

Fig. 25 : Static port experimental results for the 747 Pitot tubes (unblocked).

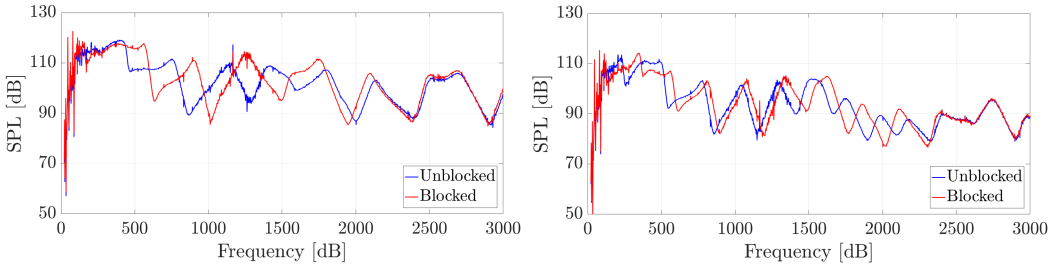

(a) 737, tube 1

(b) 747, tube 1

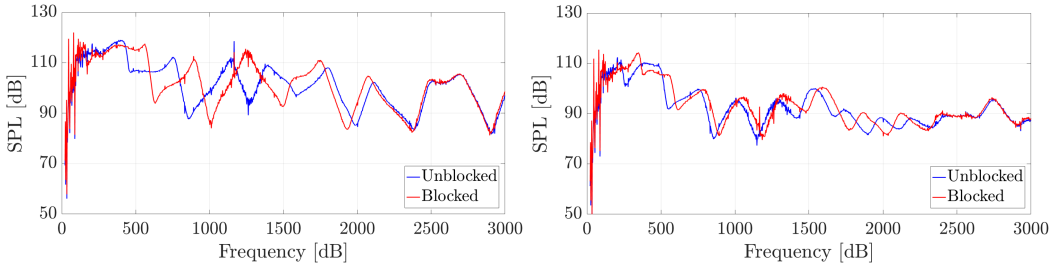

(c) 737, tube 2

(d) 747, tube 2

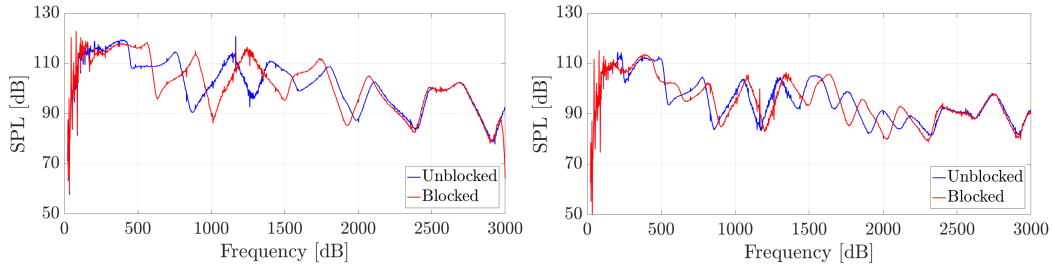

(e) 737, tube 3

(f) 747, tube 3

Fig. 26 : 737 and 747 static port experimental results.

VII. Analytical model

Consideration of an analytical acoustic model is able to explain the coalescence of the blocked and unblocked responses at higher frequencies. The pressure at the measurement location may be written as a sum of the incident wave, p_i, from the speaker and the wave reflected back from the Pitot head or static port, p_r, as:

$$p = p_i e^{j(\omega t - kx)} + p_r e^{j(\omega t + kx)} \tag{7}$$

where the wavenumber, $k = \frac{\omega}{c}$, ω is frequency and c speed of sound. In addition, the linearised inviscid momentum equation may be considered at the Pitot open end across the slits:

$$\frac{\partial u}{\partial t} = -\frac{\nabla p}{\rho} \tag{8}$$

Substituting Eq. (7) in to Eq. (8) and integrating gives:

$$u = \frac{p_i}{\rho c} e^{j(\omega t - kx)} - \frac{p_r}{\rho c} e^{j(\omega t + kx)} \tag{9}$$

Using $z = \frac{p}{u}$ at $x = L$, gives a link to the impedance:

$$z = \frac{p}{u} = \rho c \frac{p_i e^{-jkL} + p_r e^{jkL}}{p_i e^{-jkL} - p_r e^{jkL}} \tag{10}$$

where u is the velocity. With $p_i = 1$ applied to Eq. 10:

$$p_r = \frac{\frac{z}{\rho c} - 1}{e^{2jkL}\left(1 + \frac{z}{\rho c}\right)} \tag{11}$$

For a fully blocked end, $z \to \infty$, so $p_r \to e^{-2jkL}$.

The dependence of impedance on frequency can be gauged by returning to a harmonic version of equation (8) (with viscosity re-introduced for the sake of argument, and $u = u_0 e^{j\omega t}$, $p = p_0 e^{j\omega t}$, and considering only the end of the tube):

$$j\omega u_0 = -\frac{\nabla p_0}{\rho} + \nu \nabla^2 u_0 \tag{12}$$

and comparing this to $zu = p$. Qualitative consideration of this result suggests that, in the complex plane, inertial effects represent an imaginary contribution to the impedance that is (at least) proportional to the frequency, while viscous effects represent a real contribution that does not appear frequency dependent, and which will eventually become negligible, in comparison, as frequency rises.

This reasoning is supported by the detailed analysis of Macaskill and Tuck [42], who calculate the impedance of a screen consisting of a regular array of slits. Here, the impedance is defined as a pure imaginary number of the form:

$$z = -2j\omega\rho a C(\beta) \tag{13}$$

where ω is the angular frequency, ρ is the density, a is the slot semi-width, and C is a non-dimensional blockage coefficient. The latter is a function of the non-dimensional frequency, β, given by:

$$\beta = \frac{\omega a^2}{\nu} \tag{14}$$

where ν is the kinematic viscosity. Macaskill and Tuck show that the value of C is constant for values of $\sqrt{\beta}$ above 10 [42].

For the 737 Pitot total pressure system studied in §VI, the frequency responses are seen coalescing at $\sim$ 1.2 kHz. From the scans, the slot width was measured, $2a = 2.85$ mm (Fig. 5). Hence:

$$\beta = \frac{2\pi \times 1200 \times 0.001425^2}{1.46 \times 10^{-5}} \approx 1049 \tag{15}$$

so

$$\sqrt{\beta} \approx 32 \tag{16}$$

This means the assumption of constant C around the frequency where coalescence of blocked and unblocked responses is seen is consistent with the analysis of Macaskill and Tuck [42].

The salient feature regarding the Pitot head is therefore the presence of an element of impedance from the slits and the chamber surrounding those slits. The actual value of the impedance, or its origin, is relatively unimportant in explaining the coalescence of the blocked and unblocked responses, because as the frequency rises, the impedance will also increase. Eventually, the situation must arise where the reflected wave becomes the same as that for a fully blocked system. The precise value of impedance will alter the frequency range for which this behaviour becomes dominant. Similarly, it does not matter what the exact geometry of the Pitot head is, although it is preferable that it has a low impedance as this will increase the highest frequency that might be used, giving the greatest flexibility in design. Overall, it is sensible that if acoustic waves are to be measured returning from the Pitot head, then it is preferable to present the system with as few obstacles as possible.

VIII. Conclusions

Reflectometry works well on any pressure line that is smoothly ducted by a tube all the way to its end, whether it is a large Pitot head or a small static port. This configuration means the pressure line functions well as an acoustic waveguide. The unblocked/blocked signal variation becomes much smaller if the pressure line has an irregular shape, such as happens when the outer wall of the Pitot is used to contain the transmitted pressure, where the line is a poor waveguide. An acoustic blockage detection device therefore seems feasible for fully ducted lines, but usage on irregular ducts would require more testing to confirm, and may be impossible. Numerical models were found to be suitable for selecting a frequency range to use for detection, and for studying the effects of a progressive blockage on the frequency response, but the final data for use in detection would need to come from precise experimental results.

The repeatability of acoustic behaviour between Pitot tubes of the same design was checked for the available examples, but the results given here do not provide a large enough sample size for firm conclusions. Doubt therefore remains as to whether every Pitot would need calibration.

Individual calibration would prevent errors in the blockage detection system most effectively, as minor differences in manufacture would be compensated for. Any device would also benefit from the ability to auto-calibrate, whereby at regular intervals the baseline unblocked acoustic response could be updated. This would allow for gradual changes due to in-service wear.

A significant body of further work is required. The results shown here are encouraging for a ground operable system, but the influence of the background noise field in flight needs to be ascertained before a flight operable system could be proposed. In particular, almost nothing appears to be known about the external noise environment around the nose of a commercial aircraft in cruise (the internal environment is of course extensively measured for passenger/crew comfort). This data deficiency needs to be addressed, but will incur significant cost. An alternative would be to operate during flight in a mode where silence would indicate blockage [21], ie. if the background noise were no longer present in the Pitot line, a blockage could be implied to exist. Miniaturisation of the system needs to be explored once an acceptable bounding volume size is defined so that a single device may fit any aircraft, as space within the fuselage near the nose may often be restricted. Furthermore, the effects of blockages at locations upstream of the Pitot head should be investigated. Although solid ice tends to build up at the tip, insect nests or a solid-liquid ice mix could be present deeper inside the tube.

The precise structure of the detection algorithm also remains to be decided. Using a single frequency check may be sufficient, but scans over frequency ranges are likely to be more reliable. The sensitivity of the system needs to be specified against operational objectives; for example, it is likely that drain hole blockages can be detected, but whether this is desirable is uncertain. It is perhaps unwise to fly with drain holes blocked, but it might also be an overreaction to delay or cancel a flight because of it (aircraft routinely operate with failures according to minimum equipment lists, so this logic could also be used here). Ultimately, the system might only be advisory to the crew, with just a visual inspection required after a blockage detection.

Acknowledgements

The authors thank Weam Elsahhar for assistance with using the finite element acoustics modelling software, Dr. Yusuf Mahadik for assistance with the CT scans and Dr. Gregory Sutton, from the School of Biological Sciences, for providing the pre-deceased bees used in the Pitot experiments. This work was supported by the EPSRC impact acceleration account at the University of Bristol, and by the University of Bristol Faculty of Engineering. The data necessary to support the conclusions are included in the paper.

Appendix A: Three-dimensional FE Model — Mesh Statistics

Table 1 : Mesh statistics for blocked and unblocked numerical models.

	Blocked	Unblocked
Average element quality	0.7402	0.7415
Tetrahedral elements	583,032	615,825
Prism elements	0	5,376
Triangular elements	78,768	81,540
Quadrilateral elements	0	432
Edge elements	2,650	2,931
Vertex elements	114	126

Appendix B: Acoustic Source Characteristics

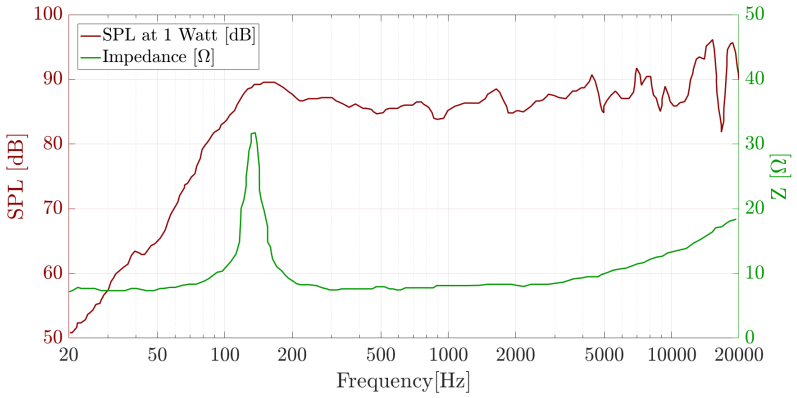

Fig. 27 : Visaton FR10-HM speaker properties [37].

Appendix C: Microphone Calibration

Calibration was conducted by comparing the FG-23329-P07 microphone's response to that of a G.R.A.S. 40PL CCP Free-field Array microphone [43]. The calibration setup was taken from Garcia [38] and Gruber [44]. The G.R.A.S. and FG-23329-P07 microphones were flush-mounted in a cap at the end of the calibration tube (labelled (a) and (b) respectively in figure 28).

Fig. 28 : Calibration setup — G.R.A.S. (a) and FG-23329-P07 (b) microphones.

The loudspeaker was at the other end connected to a cone filled with porous foam. Both pressure transducers were thus exposed to the same white noise signal. *In situ* calibration was not possible since the test setup only allowed for one microphone measurement. The calibration method was based on the procedure by Mish [45]. From this, a sensitivity file was obtained to translate the results obtained from voltage to pressure units (Fig. 29).

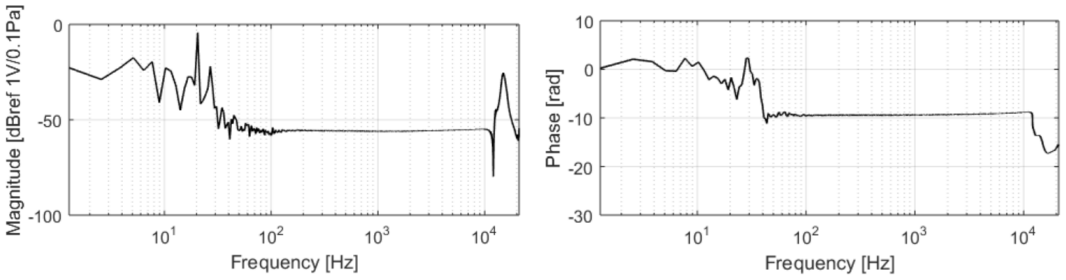

(a) FG-23329-P07 microphone level.

(b) FG-23329-P07 microphone phase.

Fig. 29 : Microphone calibration results.

References

[1] H. Pitot. Description d'une machine pour mesurer la vitesse des eaux courantes et le sillage des vaisseaux. *Histoire de l'Académie royale des sciences avec les mémoires de mathématique et de physique tirés des registres de cette Académie*, pages 363–376, 1732.

[2] H. Darcy. Note relative à quelques modifications à introduire dans le tube de Pitot. *Annales des Ponts et Chaussées*, pages 363–376, 1858.

[3] Final report on the accident on 1st June 2009 to the Airbus A330-203 registered F-GZCP operated by Air France flight AF 447 Rio de Janeiro - Paris. Technical report, Bureau d'Enquêtes et d'Analyses pour la sécurité de l'aviation Civile, 2012.

[4] Official Flight 2553 Accident Investigation Report. Technical report, Dirección Nacional de Aviación Civil e Infraestructura Aeronáutica (DINACIA) - Uruguay, December 1998.

[5] Commission of Accident Investigations (CAI). Final Report: Accident of the Aeroperú Boeing 757-200 Aircraft. Technical report, Ministry Of Transport, Communications, Housing and Construction - Director General of Air Transport (DGAT), December 1996.

[6] Final Report: Birgenair crash, Flight 301, 25th October, 1996. Technical report, DGAC Dominican Republic.

[7] Accident technical report: Northwest Airlines, Boeing 727-251, flight 6231, December 1, 1974. Technical report, National Transportation Safety Board, 1975.

[8] Jay Levine. X31's Loss. https://www.nasa.gov/centers/dryden/news/X-Press/stories/2004/013004/new_x31.html, 2004. [Online; accessed 15-May-2017].

[9] NTSB identification: DCA09IA064. Technical report, NTSB.

[10] NTSB identification: NYC05MA083. Technical report, NTSB.

[11] AAIB bulletin: 12/2009, G-STRZ, EW/A2009/01/03. Technical report, AAIB.

[12] B. Lennox D. Mackay A. R. Taylor J. T. Turner K. A. Papadopoulou, M. N. Shamout and X. Wang. An

evaluation of acoustic reflectometry for leakage and blockage detection. *Part C: Journal of Mechanical Engineering Science*, 222(6):959–966, 2008.

[13] J. L. A. Vidal and L. L. Silva. Acoustic reflectometry for blockage detection in pipeline. Offshore Technology Conference, Brasil, 29-31 October, Rio de Janeiro, Brazil, 2013.

[14] S. W. Rienstra. *Topics in Engineering Mathematics*, volume 81, chapter 8, pages 151–179. Springer Netherlands, 1st edition, 1992.

[15] D. Ramachandran and M. B. Prabhu. Acoustic sensors to detect clogs in sewer pipelines. *International Journal of Communication Network Security*, 2(2):17–19, 2013.

[16] K. V Horoshenkov M. T. Bin Ali and S. J. Tait. Detection of sewer defects and blockages using acoustic based instrumentation. *Water Science Technology*, 64(8):1700–1707, 2011.

[17] C. Hellier. *Handbook of Nondestructive Evaluation*, chapter 7. Ultrasonic Testing. McGraw-Hill, 2003.

[18] M. A. Domis. Acoustic resonances as a means of blockage detection in sodium-cooled fast reactors. *Nuclear Engineering and Design*, 54(1):125–147, 1979.

[19] D.W. Teele and J. Teele. Detection of middle ear effusion by acoustic reflectometry. *Journal of Pediatrics*, 104(6):832–838, 1984.

[20] P. H. Jarreau, B. Louis, L. Desfrère, P. W. Blanchard, D. Isabey, A. Harf, and G. Moriette. Detection of positional airway obstruction in neonates by acoustic reflection. *American Journal of Respiratory and Critical Care Medicine*, 161(5):1754–1756, 2000.

[21] N. P. Haddock. GB 2478522 B Aircraft Pitot/static warning system. UK Patent, October 2013. Cites patents GB 2191860 A, WO 2003/048713 A1, JP 590085953 A, US 4811595 A, US 20050193818 A1, EP 2273275 A1, WO 2001/091843 A1, US 5331967 A, US 20070280046 A1.

[22] R.M. Muñioz, H.W. Mocker, and L. Koehler. Airborne laser Doppler velocimeter. *Applied Optics*, 13(12):2890–2898, 1974.

[23] H.W. Mocker and T.J. Wagener. Laser Doppler optical air-data system: feasibility demonstration and systems specifications. *Applied Optics*, 33(27):6457–6471, 1993.

[24] R. Bogue, R. McGann, T. Wagener, J. Abbiss, and A. Smart. Comparative optical measurements of airspeed and aerosols on a DC-8 aircraft. Technical Report Technical Memorandum 113083, NASA, 1997.

[25] R. Bogue and H.W. Jentink. Optical Air Flow Measurements in Flight. Technical Report NASA/TP-2004-210735, NASA, 2004.

[26] S. M. Hannon, H. R. Bagley, and R. K. Bogue. Airborne Doppler lidar turbulence detection: ACLAIM flight test results. In Gary W. Kamerman; Christian Werner, editor, *Volume 3707: Laser Radar Technology and Applications IV*. Proeedings of SPIE - The International Society for Optical Engineering, 1999.

[27] B. Augere, B.. Besson, D. Fleury, D. Goular, C. Planchat, and M. Valla. 1.5 μm lidar anemometer for true air speed, angle of sideslip, and angle of attack measurements on-board Piaggio P180 aircraft. *Measurement Science and Technology*, 27(5), 2016.

[28] NEw Standby Lidar Instrument (NESLIE). Technical Report Project 30721, EU (FP6), 2010.

[29] M. B. Rhudy, M. L. Fravolini, Y. Gu, M. R. Napolitano, S. Gururajan, and H. Chao. Aircraft model-independent airspeed estimation without pitot tube measurements. *IEEE Transactions on Aerospace and Electronic Systems*, 51:1980–1995, 2015.

[30] C.A. Schneider, W.S. Rasband, and K.W. Eliceiri. NIH Image to ImageJ: 25 years of image analysis. *Nature Methods*, 9:671–675, 2012.

[31] T. Swafford, J. Bomba, and M. Daiber. Computational analysis of compensated Pitot-static probes using the Euler equations. AIAA, Proc. 13th AIAA Applied Aerodynamics Conference, San Diego, CA, June 19-22,1995, 1995. Paper number AIAA-1995-1839.

[32] COMSOL Multiphysics User's Guide Version 4.3. Technical report, COMSOL, 2012.

[33] Steffen Marburg. *Computational Acoustics of Noise Propagation in Fluids - Finite and Boundary Element Methods*, chapter 11. Discretization Requirements: How many Elements per Wavelength are Necessary?, pages 309–332. Springer Berlin Heidelberg, 2008.

[34] A. Bidgoli, J. de Souza, K. Lisboa, and R. Cotta. Thermal analysis of heated Pitot probes in atmospheric conditions of ice accretion. ABCM, 23rd ABCM International Congress of Mechanical Engineering December 6-11, 2015, Rio de Janeiro, RJ, Brazil, 2015.

[35] J.-P. Berenger. A perfectly matched layer for the absorption of electromagnetic waves. *Journal of Computational Physics*, 114(2):185–200, 1994.

[36] E. Holzbecher and H. Si. Accuracy tests for comsol - and Delaunay meshes. Proceedings of the COMSOL Conference 2008 Hannover, January 2008.

[37] Visaton FR 10 HM - 8 Ohm Technical Data. http://www.visaton.com/en/chassis_zubehoer/breitband/fr10hm_8.html, 2015. [Online; accessed 20-July-2016].

[38] Ana Garcia Sagrado. *Boundary Layer and Trailing Edge Noise Sources*. PhD thesis, Whittle Laboratory, Department of Engineering, University of Cambridge, December 2007.

[39] H. Kuttruff. *Acoustics: An Introduction*. CRC Press, 2006. Chapter 4: Plane waves, attenuation.

[40] A. D. Pierce and P. W. Smith. *Acoustics: An Introduction to Its Physical Principles and Applications*, volume 34 of *10*. McGraw-Hill Book Company, 1st edition, January 1981. Chapter 10: Effects of Viscosity and Other Dissipative Processes.

[41] P. Juhl R. Christensen and V. Cutanda Henriquez. Practical modeling of acoustic losses in air due to heat conduction and viscosity. *The Journal of the Acoustical Society of America*, 123(5), 2008.

[42] C. Macaskill and E.O. Tuck. Evaluation of the acoustic impedance of a screen. *The Journal of the Australian Mathematical Society Series B Applied Mathematics*, 20:46–61, 1977.

[43] G.R.A.S. Sound and Vibration. G.R.A.S. 40PL CCP Free-field Array Microphone, High Pressure. March 2012.

[44] Mathieu Gruber. *Airfoil noise reduction by edge treatments*. PhD thesis, University of Southampton, February 2012.

[45] Patrick F. Mish. *Mean Loading and Turbulence Scale Effects on the Surface Pressure Fluctuations Occurring on a NACA 0015 Airfoil Immersed in Grid Generated Turbulence*. PhD thesis, Virginia Polytechnic Institute and State University, May 2001.